Journal of Wind Engineering & Industrial Aerodynamics 254 (2024) 105901

Contents lists available at ScienceDirect

Journal of Wind Engineering & Industrial Aerodynamics

journal homepage: www.elsevier.com/locate/jweia

A comparative study on the crosswind stability of the railway vehicle considering distinct national standards

Dongqin Zhang [a], Takeshi Ishihara [b,*]

[a] Department of Civil and Environmental Engineering, The Hong Kong University of Science and Technology, Hong Kong, China
[b] Department of Civil Engineering, School of Engineering, The University of Tokyo, Tokyo, Japan

ARTICLE INFO

Keywords:
Railway vehicle
Crosswind stability
Track irregularities
Characteristic wind curve (CWC)
Quasi-static analysis (QSA)
Multibody simulations (MBS)

ABSTRACT

The crosswind stability of railway vehicles, considering distinct national standards in both quasi-steady and unsteady wind conditions, like Chinese hat gust wind (EN 14067-6, 2010), is systematically evaluated. Initially, it is observed that the quasi-static analysis (QSA) proposed in Japan marginally underestimates the wheel unloading ratio of railway vehicles by approximately 3 %, as the external forces increase beyond a certain threshold in quasi-steady winds due to the neglect of the vertical degree of freedom and the inability to accurately evaluate the activation of vertical bump stops. Subsequently, to accurately assess the crosswind responses of railway vehicles under realistic conditions, a non-linear lateral acceleration model is proposed to account for the effects of track irregularities, validated against field test data. Finally, it is noted that the Chinese standard is more conservative, with characteristic wind speeds (CWC) approximately 2 m/s lower than those calculated by the European standard, while the Japanese guideline is more stringent at high train velocities but more lenient at low velocities. The CWC evaluated under gust wind conditions is around 2.4 m/s higher than those obtained under quasi-steady winds, due to the maximum gust wind speed is low-pass filtered by the centered moving average method.

1. Introduction

Crosswinds pose a significant threat to the running safety of railway vehicles, potentially leading to overturning or derailment (Baker et al., 2009). Fig. 1 illustrates railway accidents caused by strong winds in Japan, China, Europe, and the United States. Japan, China, and Europe have developed their own standards or regulations (Hibino et al., 2010a; GB5599-85, 1985; EN 14067-6, 2010) for assessing the safety of railway vehicles under high wind conditions, but significant differences exist in the train models, methods for accounting for track irregularities, and safety criteria used across these regions. To date, a comprehensive evaluation comparing these diverse approaches has not been conducted.

Dynamic responses of railway vehicles are typically calculated using either quasi-static analysis (QSA) or multibody simulations (MBS) following the evaluation of external forces (Baker, 2013). In Europe, quasi-static methods, including the simple three-mass model and the more complex five-mass model (Diedrichs et al., 2004), are employed to assess crosswind responses of railway vehicles due to their simplicity. Additionally, MBS are utilized to evaluate crosswind responses under Chinese hat gust winds (EN 14067-6, 2010) and unsteady winds (Thomas et al., 2010). In China, MBS is widely adopted for calculating the dynamic response of trains subjected to both quasi-steady and unsteady winds (Liu et al., 2020; Zhang et al., 2023). In Japan, the quasi-static analysis with 3 degrees of freedom (3DoFs) and a half-car model proposed by Hibino et al. (2010b) is broadly used to calculate characteristic wind curves (CWC) for commuter rails (Misu and Ishihara, 2012, 2018). A full railway vehicle model with 31 degrees of freedom has also been proposed to evaluate gust wind effects (Hibino et al., 2010a), though it is not widely adopted by railway companies in Japan. Comparative studies, such as those between MBS and the three-mass model under Chinese hat gusts (Sesma et al., 2012), have shown that the characteristic wind curve calculated by the three-mass model aligns well with results obtained via MBS. The effects of rail vehicle properties on crosswind stability have been examined by Heleno et al. (2021). Furthermore, comparisons between MBS and QSA under tunnel exit winds (Ishihara et al., 2021) and tornado winds (Zhang and Ishihara, 2022) reveal that QSA underestimates the maximum unsteady crosswind response in Japan. However, a systematic comparison of QSA and MBS under quasi-steady winds and Chinese hat gusts has not been conducted.

* Corresponding author.
E-mail address: ishihara@bridge.t.u-tokyo.ac.jp (T. Ishihara).

https://doi.org/10.1016/j.jweia.2024.105901
Received 24 August 2024; Received in revised form 16 September 2024; Accepted 17 September 2024

In order to accurately assess the dynamic responses of railway vehicles under crosswinds, it is crucial to consider the effects of track irregularities. Generally, three methods are employed to account for these effects. Firstly, a critical situation induced by crosswinds is defined by a 90 % wheel unloading threshold, with the remaining 10 % serving as a safety margin for track irregularities. This approach is commonly used in Europe (EN 14067-6, 2010). Secondly, track irregularities can be simulated using power spectral density (PSD) methods, such as the German high/low-disturbance spectrum (Zhang et al., 2016), or simplified periodic irregularities (Claus and Schiehlen, 1998; Montenegro et al., 2022). This method is widely adopted for modeling train-bridge interactions under crosswinds using multibody simulations. Thirdly, in Japan, the linear lateral acceleration model (LLAM) is applied to account for track irregularities when evaluating critical wind curves using quasi-static approaches (QSA) (Hibino et al., 2010b). However, the LLAM tends to overestimate lateral accelerations at high running velocities and underestimate them at lower velocities, compared to field measurements. In fact, the overturning of a railway vehicle has occurred as the train velocity maintains around 25 km/h which means that it is essential to evaluate effects of track irregularities accurately even for the case with a low train velocity (ARAIC, 2008). Consequently, the LLAM's limitations highlight the need for a more precise lateral acceleration model that can account for varying train velocities.

The evaluation criteria for train overturning due to crosswinds vary significantly across different regions. In China, the primary criterion for assessing crosswind stability is the overturning coefficient, with a critical value set at 80 % (GB5599-85, 1985; Liu et al., 2019; Zhang et al., 2024). In Europe, the wheel unloading ratio is used, with a critical threshold of 90 % (EN 14067-6, 2010; Baker, 2013). Japan employs a similar criterion but sets the critical value at 100 %, taking into account the lateral force induced by track irregularities when calculating the dynamic responses of railway vehicles (Hibino et al., 2010b; Misu and Ishihara, 2018). Table 1 illustrates the evaluation methods, criteria, and critical values across these regions, highlighting the distinct differences.

Table 1
Comparisons of methods to evaluate the crosswind stability of railway vehicle in different regions.

Region	Vehicle models	Track irregularity	Criteria	Critical values
China	MBS	No	Overturning coefficient	80 %
Europe	MBS QSA in Europe	No	Wheel unloading ratio	90 %
Japan	QSA in Japan	Lateral force	Wheel unloading ratio	100 %

This study provides a comprehensive comparison of the crosswind stability of railway vehicles evaluated in different regions, encompassing various factors such as train models, track irregularities, criteria, and critical values. Both quasi-steady winds and Chinese hat gusts are considered in the analysis.

High-speed railway networks are being developed across various countries by different constructors, such as Japan in India and China in Indonesia, yet there is currently no international standard for assessing the safety of railway vehicles under crosswind conditions. This study seeks to address this gap by comparing the methods and criteria employed in different national regulations and offering recommendations for evaluating the crosswind stability of railway vehicles.

2. Numerical models

Section 2.1 interprets different wind scenarios, including the quasi-steady wind and the Chinese hat gust. The non-linear lateral acceleration model induced by track irregularities is proposed in section 2.2. The quasi-static analysis and the multibody simulation of railway vehicle are presented in section 2.3 and section 2.4, respectively. Finally, the evaluation criteria are described in section 2.5.

Fig. 1. Derailment or overturning accidents by strong winds all over the world (a) in Japan, (b) in China, (c) in Switzerland and (d) in the USA.

2.1. Wind scenarios and aerodynamic forces

Fig. 2 depicts the quasi-steady wind scenario, where wind speed increases linearly from zero to a constant value over the first 10 s and then remains constant for the subsequent 20 s. During this period, it is assumed that the wind speed holds steady at this constant value and that turbulence intensity is negligible.

Additionally, the Chinese hat gust model (EN 14067-6, 2010) is employed to simulate turbulent wind conditions. For railway vehicles, this model, with its biexponential shape, is typically used to evaluate characteristic wind curves. It is defined by a gust factor of 1.6946 and can be expressed as follows:

$$G = \frac{U_{\max}}{\overline{U}} \tag{1}$$

where $\overline{U}$ and $U_{\max}$ stand for the mean and maximum wind speeds.

The gust factor is derived from a roughness length of 0.07 m and a height of 4 m above the terrain, corresponding to a turbulence intensity of 0.2446.

Another crucial parameter of the gust model is the characteristic frequency f, which is defined as follows:

$$f = \frac{1}{2\overline{T}}, T = 4.1825\overline{T} \tag{2}$$

where $\overline{T}$ refers to the time constant of gust duration. It can be expressed as follows:

$$\overline{T} = \frac{1}{2}\left[\frac{\int_{n_1}^{n_2} n^2 S_u(n)dn}{\int_{n_1}^{n_2} S_u(n)dn}\right]^{-0.5} \tag{3}$$

where n_1 and n_2 are the lower and upper limitations of frequency and they are assumed to be 1/300 Hz and 1 Hz, respectively, the frequency range $n \in [n_1, n_2]$, $S_u(n)$ shows the von Kármán PSD which is defined as follows:

$$S_u(n) = \frac{4f_u\sigma_u^2}{\left[1 + 70.7f_u^2\right]^{5/6}}\frac{1}{n} \tag{4}$$

where σ_u and f_u represent the standard deviation and the normalized frequency. They can be expressed as follows:

$$\sigma_u = 0.2446\overline{U} \tag{5}$$

$$f_u = \frac{nL_n}{\overline{U}} \tag{6}$$

where L_n presents the integral length scale and it is defined as 96.0395 m.

The wind speed spatially distributed along the track can be calculated as follows:

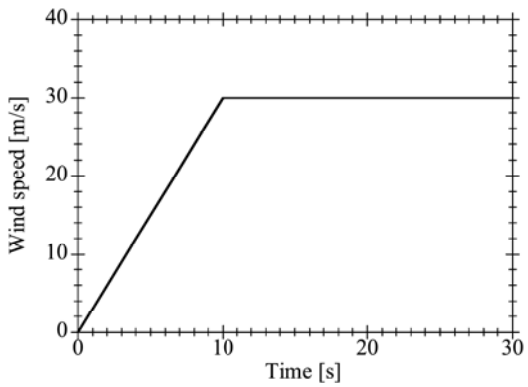

Fig. 2. Descriptions of the quasi-steady wind scenario.

$$U(x) = \overline{U} + 2.84\sigma_u e^{\frac{-16f\cdot x}{\overline{U}}} \tag{7}$$

where x shows the longitudinal distance towards the position of the gust peak.

As the railway vehicle runs along the track, the centered moving average method is employed to transform the spatial wind speed to the temporal wind speed, and it can be expressed as follows:

$$v_c = \frac{\int_{\left(V_{tr}-\frac{L_0}{2}\right)}^{\left(V_{tr}+\frac{L_0}{2}\right)} U(x)dx}{L_0} \tag{8}$$

where L_0 refers to the carriage length, v_c present the temporal wind speeds, t is time, V_{tr} represents the train velocity.

In both spatial and temporal domains, the wind speed increases linearly to reach the mean wind speed, maintaining the constant value over a certain distance in Fig. 3. Subsequently, the wind speed rises exponentially to its maximum value before decreasing in a similar manner. The wind direction is perpendicular to the track, at 90°. Notably, the maximum wind speed in the temporal domain is lower than that in the spatial domain, as it accounts for the wind distribution along the entire carriage.

Considering the train velocity and the angle of wind attack, the relative wind direction $\beta(t)$ and resultant wind speed $v_a(t)$ are determined through Eq. (9) and Eq. (10), as depicted in Fig. 4(a). Aerodynamic forces on the carriage are computed by the quasi-steady theory, as illustrated in Fig. 4(b). Previous studies (Ishihara et al., 2021) have demonstrated that both the quasi-steady theory and the equivalent wind force approach can reliably predict the aerodynamic forces induced by crosswinds on railway vehicles.

$$\beta(t) = \arctan\left(\frac{v_c(t)\sin\beta_w}{V_{tr} + v_c(t)\cos\beta_w}\right) \tag{9}$$

$$v_a(t) = \sqrt{\left[V_{tr} + v_c(t)\cos\beta_w\right]^2 + \left[v_c(t)\sin\beta_w\right]^2} \tag{10}$$

$$F_S(t) = \frac{1}{2}\rho A C_S(\beta(t))v_a^2(t) \tag{11}$$

$$F_L(t) = \frac{1}{2}\rho A C_L(\beta(t))v_a^2(t) \tag{12}$$

$$M_R(t) = \frac{1}{2}\rho A C_M(\beta(t))v_a^2(t)H_0 \tag{13}$$

where $v_c(t)$ and β_w present the temporal wind speed at carriage center, $F_S(t)$, $F_L(t)$ and $M_R(t)$ represent side and lift forces, and rolling moment, ρ is the air density, H_0 and A show the height and side area of car body, C_S, C_L and C_M represent the aerodynamic coefficients (Fig. 5) as measured in the wind tunnel at the University of Tokyo, which are defined by the following equations. A 1:40 scale model of the train, including the first and second carriages, was positioned on a bridge, with aerodynamic forces captured using a six-component force balance. The experiments were conducted under atmospheric boundary layer (ABL) inflow conditions, characterized by a power-law exponent of 1/7 and a turbulence intensity of approximately 15 % at the vehicle's center height (Nagumo and Ishihara, 2019).

$$C_S = \frac{F_S}{\frac{1}{2}\rho A v_a^2} \tag{14}$$

$$C_L = \frac{F_L}{\frac{1}{2}\rho A v_a^2} \tag{15}$$

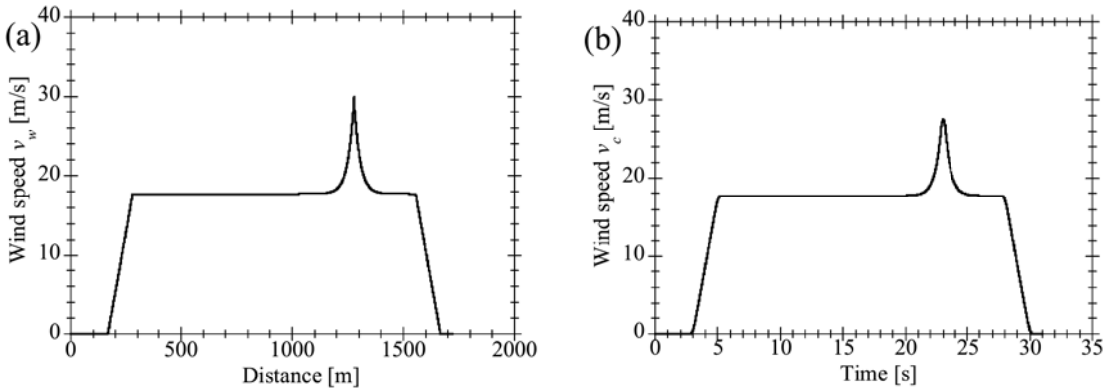

Fig. 3. Descriptions of (a) the spatial and (b) the temporal Chinese hat gust model.

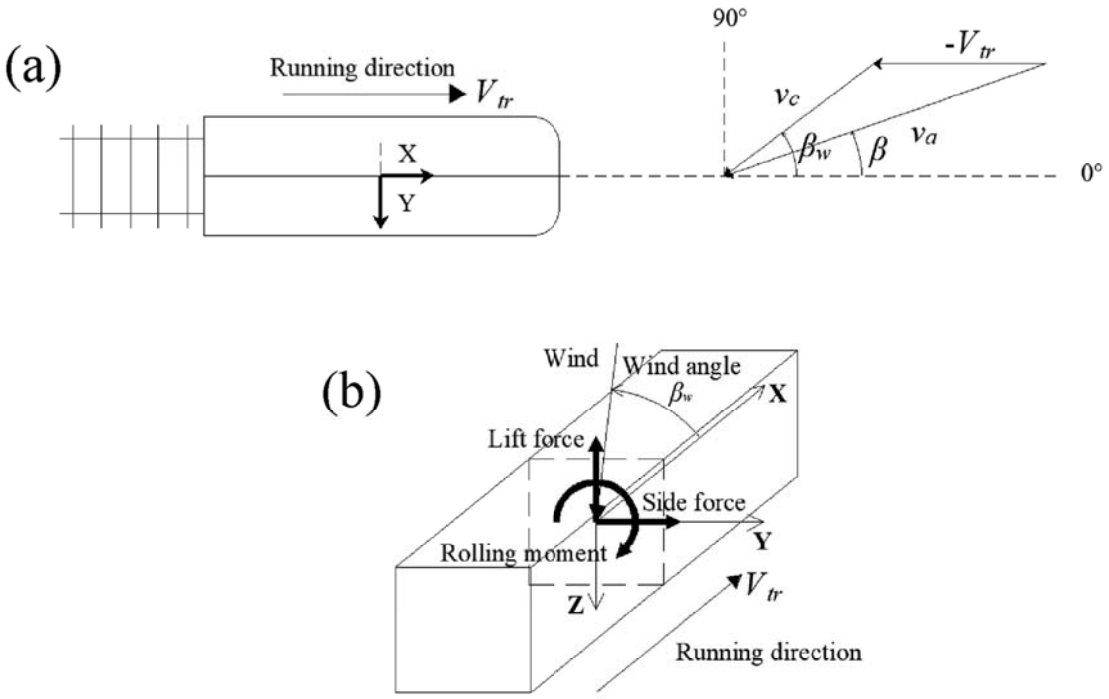

Fig. 4. Directions of (a) crosswinds and (b) aerodynamic forces.

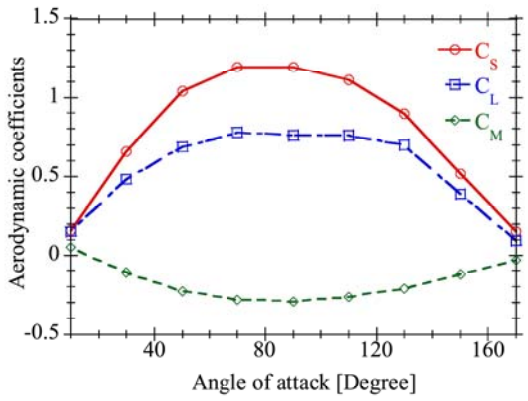

Fig. 5. Aerodynamic coefficients measured in the wind tunnel.

$$C_M = \frac{M_R}{\frac{1}{2}\rho A v_a^2 H_0} \tag{16}$$

2.2. Lateral acceleration model induced by track irregularities

In Japan, the linear lateral acceleration model is employed to simulate track irregularities, with the variation in acceleration data as a function of train speed presented in Fig. 6. This model, proposed by Hibino et al. (2010b), is used to simulate the effects of track irregularities when calculating the characteristic wind curve for train overturning. The lateral force, determined by the relationship $F = ma$, is applied to the railway vehicle. In this study, we propose a non-linear lateral acceleration model that considers the effects of track irregularities. This model increases linearly until the train velocity reaches 20 km/h, after which it maintains a constant value (0.6 in this study) for velocities equal to or exceeding 20 km/h. It is assumed that the vibration caused by track irregularities does not vary with train velocity beyond 20 km/h. Both the linear and non-linear lateral acceleration models are depicted in Fig. 6.

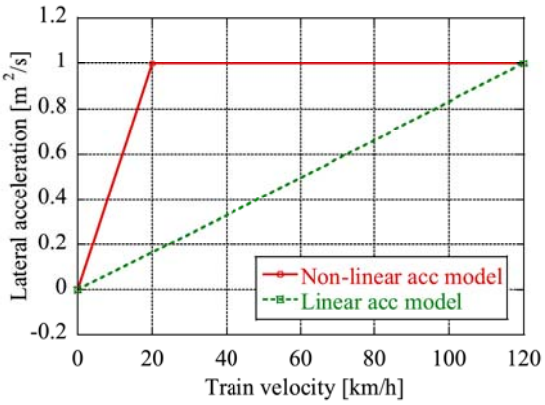

Fig. 6. The lateral acceleration models to consider the effect of track irregularities.

2.3. Quasi-static analysis in Japan

Hibino et al. (2010b) proposed a quasi-static analysis model with three degrees of freedom (3DoFs), representing a 2D vehicle model as illustrated in Fig. 7. This approach is widely used in Japan to evaluate characteristic wind curves for train overturning. The 3DoFs account for the primary deformations of the car body, including the rolling angles relative to the first and second suspension systems (ϕ_1, ϕ_2), and the lateral displacement about the second suspension system (y_2). These variations enable the determination of the main deformations of the car body, encompassing rolling angles, and lateral and vertical displacements.

The three degrees of freedom are resolved using the minimum potential energy principle, and the wheel loading on the leeward side is derived from the static equilibrium equation.

$$D_{WR}P_L = m_T g\frac{G}{2} + \frac{m_B}{2}g\left(\frac{G}{2} - y_B\right) - F_L\left(\frac{G}{2} - y_B + e\phi_B\right) - h_{GT}F_u' - h_{GB}(F_u + F_V) - h_{BC}F_S \quad (17)$$

where P_L is the windward wheel loading, D_{WR} shows the distance between two wheel-rail contact points, h_{BC} and h_{GB} exhibit the heights of wind pressure centre and the gravity centre, respectively, e can be expressed as $e = h_{BC} - h_{GB}$, F_u, F_u' and F_V display external forces, namely, the side force, the lift force, excessive centrifugal forces, and the lateral force considering the effects of track irregularities, g shows the gravitational acceleration.

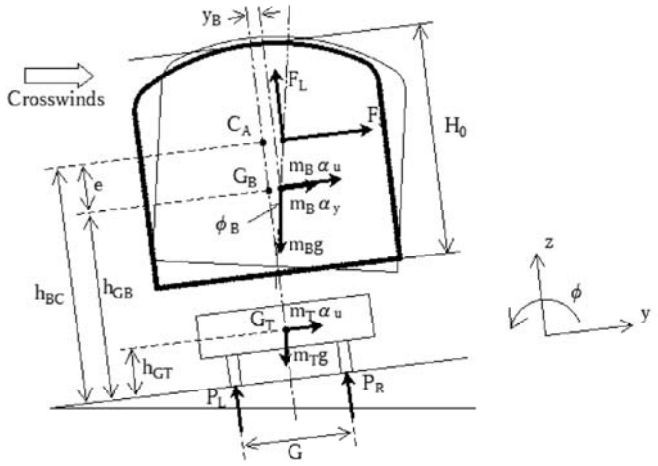

Fig. 7. A 2D half-car model in QSA.

2.4. Multibody simulation

The MBS approach is employed to investigate the crosswind stability of railway vehicles by constructing a full vehicle model, where each component is interconnected by the primary and secondary suspension systems, as depicted in Fig. 8. Each rigid body in the model possesses six degrees of freedom, resulting in a total of 42 DoFs for the entire train model. The 6 DoFs of the car body encompass the motions and the rotational motions along three main axial directions, denoted as $\{v_c\} = \{x_c, y_c, z_c, \varphi_c, \theta_c, \psi_c\}^T$. Likewise, the i-th bogie and j-th wheelset possess their respective DoFs, represented as $\{v_{bi}\} = \{x_{bi}, y_{bi}, z_{bi}, \varphi_{bi}, \theta_{bi}, \psi_{bi}\}^T$ and $\{v_{wij}\} = \{x_{wij}, y_{wij}, z_{wij}, \varphi_{wij}, \theta_{wij}, \psi_{wij}\}^T$. The DoFs of the whole carriage model can be expressed as $\{v_t\} = \{v_c, v_{b1}, v_{b2}, v_{w11}, v_{w12}, v_{w23}, v_{w24}\}^T$. The suspension systems incorporate longitudinal, lateral, and vertical springs and dampers, along with non-linear lateral bump stops and anti-snake dampers, linking the wheelsets, bogies, and car body. Kalker's FASTSIM algorithm is employed to compute the wheel/rail contact forces. The vehicle's equations of motion are formulated as:

$$[M_t]\{\ddot{v}_t\} + [C_t]\{\dot{v}_t\} + [K_t]\{v_t\} = \{f_t\} \quad (18)$$

where $\{f_t\}$ are the external forces, $[M_t]$, $[K_t]$ and $[C_t]$ represent the matrix of mass, stiffness and damping terms of the train which are not illustrated in this study and can be found by Su et al. (2010), Zhai et al. (2013), Ishihara et al. (2021).

2.5. Evaluation criteria for crosswind stability of railway vehicle

The wheel unloading ratio is utilized as a key index to evaluate the risk of railway vehicle overturning under crosswind conditions in both Japan (Hibino et al., 2010b) and Europe (EN 14067-6, 2010). The critical values for this index are 100 % in Japan and 90 % in Europe, reflecting the inclusion of track irregularities in the Japanese assessment, which increases the critical threshold compared to the European standard. It is defined as follows:

$$D = \frac{P_0 - P_L}{P_0} \quad (19)$$

where P_0 and P_L display the static and windward wheel loadings.

In China, the criterion for assessing the crosswind stability of a railway vehicle is the overturning coefficient D'. Unlike the wheel unloading ratio, which considers the actual wheel unloading in its denominator, D' accounts for this value adjusted by the lift force generated by crosswinds, resulting in slightly different calculated values between the two criteria. To maintain the safety of railway vehicles under crosswind conditions, the overturning coefficient is limited to remain below 0.8 (GB5599-85, 1985).

$$D' = \frac{P_R - P_L}{P_R + P_L} \quad (20)$$

where P_R stands for the wheel loading on the leeward side.

The relationship between the wheel unloading ratio and the overturning coefficient is established based on the distinction between dynamic and static wheel loadings. The dynamic (P_0') and static (P_0) wheel loadings are defined as follows:

$$P_0 = (F_L + P_R + P_L)/2 \quad (21)$$

$$P_0' = (P_R + P_L)/2 \quad (22)$$

The sum of the dynamic wheel loading and the lift force equals the static wheel loading, indicating that the dynamic wheel loading is less than the static counterpart. The relationship between the wheel

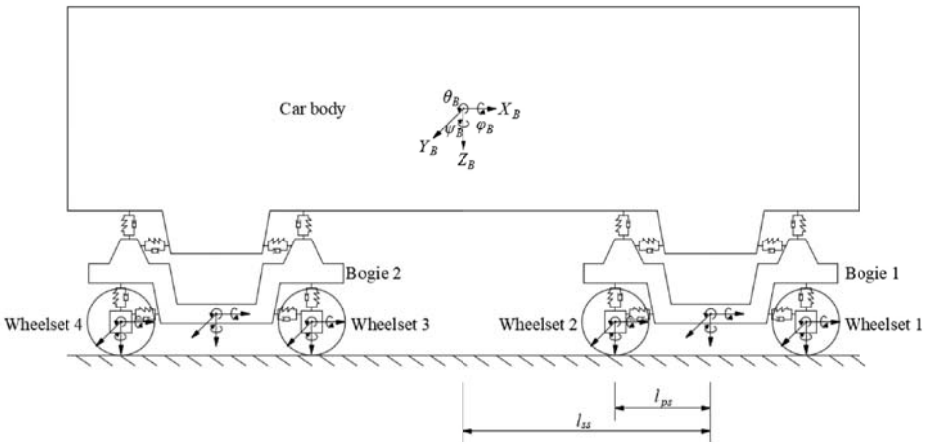

Fig. 8. A full vehicle model in MBS.

unloading ratio of the entire vehicle and the overturning coefficient can be formulated as follows:

$$D' = D\frac{\left(2{P_0}^2 - P_0F_L - 2P_LP_0\right)}{\left(2{P_0}^2 - P_0F_L - 2P_LP_0 + F_LP_L\right)} \tag{23}$$

An additional term in the denominator (F_LP_L), is observed, resulting in the overturning coefficient being slightly lower than the wheel unloading ratio.

3. Results and discussions

Quantitative comparisons of QSA and MBS under quasi-steady winds and Chinese hat gusts are presented in section 3.1. In section 3.2, we investigate track irregularity, followed by an analysis of evaluation criteria in section 3.3. Finally, section 3.4 compares the characteristic wind curves obtained through different national standards.

3.1. Comparison of the results of the QSA and MBS analysis

Numerical models of the commuter rail (E233 series) were developed using QSA and MBS methodologies as shown in Ishihara et al. (2021). Field tests, conducted by the East Japan Railway Company, validated the accuracy of these railway vehicle models, with detailed experimental procedures described in Appendix A.

As illustrated in Table 2, six distinct train speeds were analyzed. For each train speed, 23 quasi-steady wind speeds ranging from 10 m/s to 32 m/s are considered, with 1 m/s intervals, resulting in a total of 138 cases. The variation in quasi-steady wind speed is depicted in Fig. 2, while the aerodynamic forces for a train speed of 120 km/h and a wind speed of 30 m/s are illustrated in Fig. 9.

Subsequently, the dynamic responses of the railway vehicle under quasi-steady wind conditions, calculated using QSA and MBS, are compared. Fig. 10 illustrates lateral and vertical displacements, the rolling angle of the car body, and the wheel unloading ratio. It is observed that lateral displacement and rolling angle calculated by both methods are closely aligned at a wind speed of 10 m/s, while the values

Table 2
Description of simulation cases under quasi-steady winds.

Cases	Train velocity [km/h (m/s)]	Quasi-steady wind speeds [m/s]
1–23	20 (5.56)	10~32 at the interval of 1
24–46	40 (11.11)	10~32 at the interval of 1
47–69	60 (16.67)	10~32 at the interval of 1
70–92	80 (22.22)	10~32 at the interval of 1
93–115	100 (27.78)	10~32 at the interval of 1
116–138	120 (33.33)	10~32 at the interval of 1

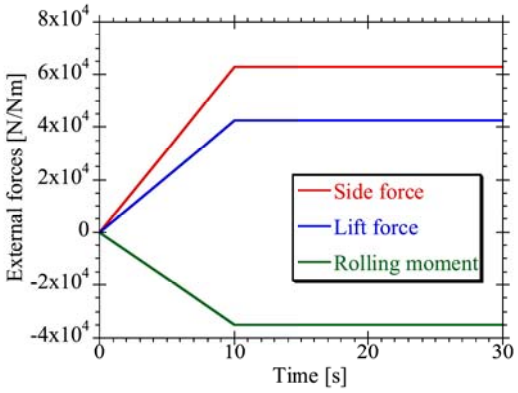

Fig. 9. Quasi-steady wind-induced aerodynamic forces with the train speed of 120 km/h and the quasi-steady wind speed of 30 m/s.

derived from multibody simulations are slightly higher at a wind speed of 30 m/s. For vertical displacements, QSA produces opposing results due to its exclusion of the vertical degree of freedom of the car body, accounting for vertical displacements through the rotation and deflection of the car body. The wheel unloading ratio obtained by both methods shows remarkable similarity at a train velocity of 20 km/h, indicating that errors arising from assumptions regarding car body displacements do not significantly affect the wheel unloading ratio at this speed. However, as the train velocity increases to 120 km/h, the wheel unloading ratio obtained by multibody simulations becomes marginally higher, owing to the quasi-static analysis neglecting the vertical degree of freedom of the car body.

Fig. 11 presents the systematic comparison results obtained using QSA and MBS under quasi-steady wind conditions. The lateral displacements and rolling angles calculated by both methods are identical and follow the line $y = x$ when the lateral displacement is below approximately 100 mm, or the rolling angle is less than about 3°. Beyond these thresholds, the values calculated by QSA decrease noticeably compared to those obtained by MBS. This discrepancy arises because QSA assumes the vertical displacement of the car body is nearly zero, causing the vertical bump stops to engage prematurely. In reality, the car body ascends under crosswinds due to lift forces, preventing the vertical bump stops from continuous engagement. However, QSA predicts a downward vertical displacement, eliminating the clearance between the car body and vertical bump stops as aerodynamic forces increase, erroneously incorporating the bump stops prematurely. This results in QSA considering an additional spring effect, potentially underestimating the dynamic responses. Conversely, MBS accurately

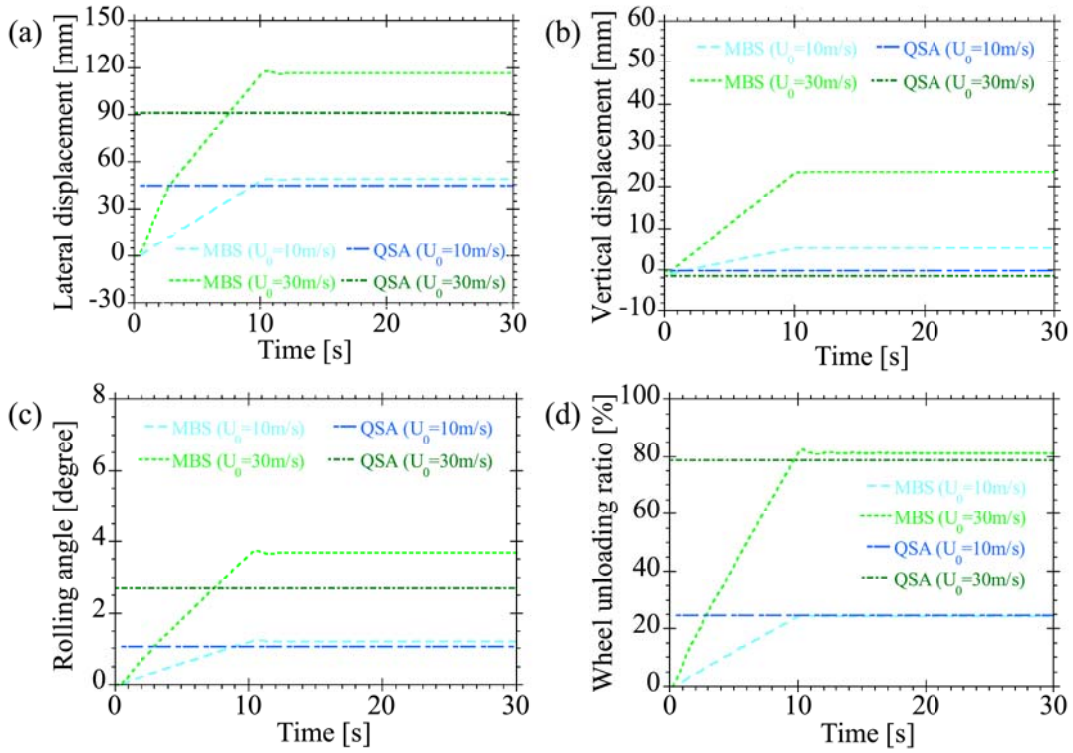

Fig. 10. Comparisons of (a) lateral displacements, (b) vertical displacements, (c) rolling angles of car body, and (d) wheel unloading ratios under quasi-steady winds with the train velocity of 120 km/h.

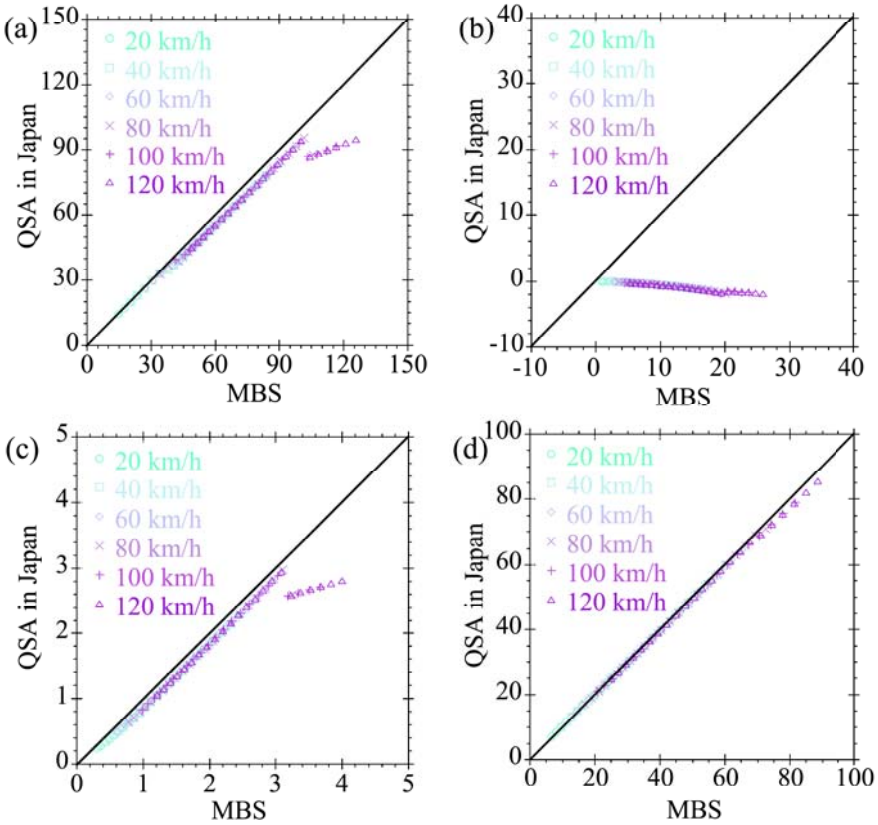

Fig. 11. Comparisons of (a) lateral displacements, (b) vertical displacements, (c) rolling angles of car body, and (d) wheel unloading ratio calculated by two approaches under quasi-steady wind conditions.

predicts the vertical displacement of the car body, aligning with real-world conditions. The wheel unloading ratio obtained by both approaches are almost identical when below 80 %, but QSA yields slightly smaller values due to the inclusion of vertical bump stops. Consequently, it is concluded that QSA marginally underestimates the dynamic responses of railway vehicles (around 3 % for the wheel unloading ratio) as aerodynamic forces increase due to the neglect of the vertical degree of freedom and the inability to accurately evaluate the activation of vertical bump stops.

Additionally, the wheel unloading ratios calculated from the wheel loading of the wheelset, bogie, and car body are compared in Fig. 12. The analysis reveals that these three wheel unloading ratios are closely aligned, suggesting that any of them can be effectively used to evaluate the crosswind stability of railway vehicles in quasi-steady winds.

To compare the results obtained by QSA and MBS under Chinese hat gust, six scenarios are considered, with train velocities ranging from 20 km/h to 120 km/h, as detailed in Table 3. For each scenario, the maximum wind speed increases from 10 m/s to 32 m/s. The distribution of the Chinese hat gust is defined by EN 14067-6, (2010) and depicted in Fig. 3. The aerodynamic forces caused by the Chinese hat gust are presented in Fig. 13. For MBS, the time series of external forces are input into the full vehicle model, allowing the direct determination of the maximum dynamic response of the commuter rail. In contrast, QSA uses the maximum wind speed to calculate the dynamic responses.

Similar to the dynamic responses of a railway vehicle in quasi-steady wind conditions, lateral and vertical displacements, rolling angle, and wheel unloading ratios obtained by QSA and MBS are compared in Fig. 14. Notably, the wheel unloading ratio is accurately assessed when the maximum spatial wind speed maintains 10 m/s, whereas other responses are underestimated by QSA. This discrepancy is particularly pronounced in the case of the Chinese hat gust.

Fig. 15 illustrates the wheel unloading ratios calculated from the wheel loading of the wheelset, bogie, and car body at various train speeds under Chinese hat gust. The results show a high degree of similarity across these different methods, suggesting that the wheel unloading ratio derived from any of these wheel loadings can be reliably adopted.

Fig. 16 resents a comparison of results calculated by QSA and MBS under Chinese hat gust conditions. Similar to the quasi-steady wind scenarios, the dynamic responses of the railway vehicle calculated by QSA are underestimated as aerodynamic forces increase, due to its inability to accurately assess the activation of vertical bump stops. Additionally, the differences in wheel unloading ratios become more pronounced as aerodynamic forces rise, compared to those observed under quasi-steady winds. It is noteworthy that QSA may underestimate the dynamic responses of railway vehicles subjected to short-rise-time gust winds. Ishihara et al. (2021) proposed the dynamic amplification factor (DAF) to evaluate this dynamic amplification effect. Consequently, it is concluded that QSA may underestimate the crosswind responses of railway vehicles in Chinese hat gust conditions due to two primary reasons: (1) the neglect of the vertical degree of freedom, and (2) the dynamic amplification effects.

Table 3
Description of simulation cases under Chinese hat gust.

Cases	Train velocity [km/h (m/s)]	Maximum wind speeds [m/s]
139–161	20 (5.56)	10~32 at the interval of 1
162–184	40 (11.11)	10~32 at the interval of 1
185–207	60 (16.67)	10~32 at the interval of 1
208–230	80 (22.22)	10~32 at the interval of 1
231–253	100 (27.78)	10~32 at the interval of 1
254–276	120 (33.33)	10~32 at the interval of 1

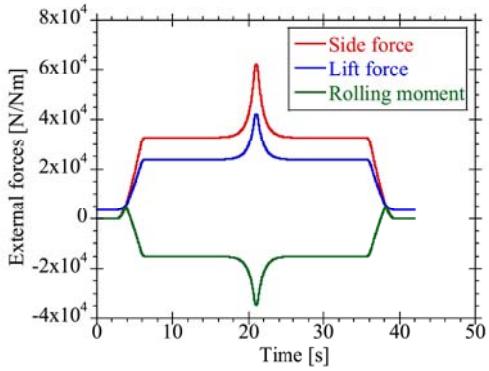

Fig. 13. Aerodynamic forces induced by Chinese hat gust with the train speed of 120 km/h and the quasi-steady wind speed of 30 m/s.

3.2. Impact of track irregularity

As shown in Fig. 17, the lateral accelerations of the car body for commuter trains, caused by track irregularities, were measured by the East Japan Railway Company (Akiko et al., 2015). To capture these accelerations, an AS-2GB accelerometer was placed at the center of the car body, while GPS was used to obtain train velocities during operation. Data were sampled at a frequency of 1 kHz, and a 2 Hz low-pass filter was applied to remove high-frequency vibrations that do not affect train overturning. Peak values were recorded at 2-s intervals along with the corresponding train velocities, resulting in a total dataset of 64,186 measurements (Nagumo and Ishihara, 2019).

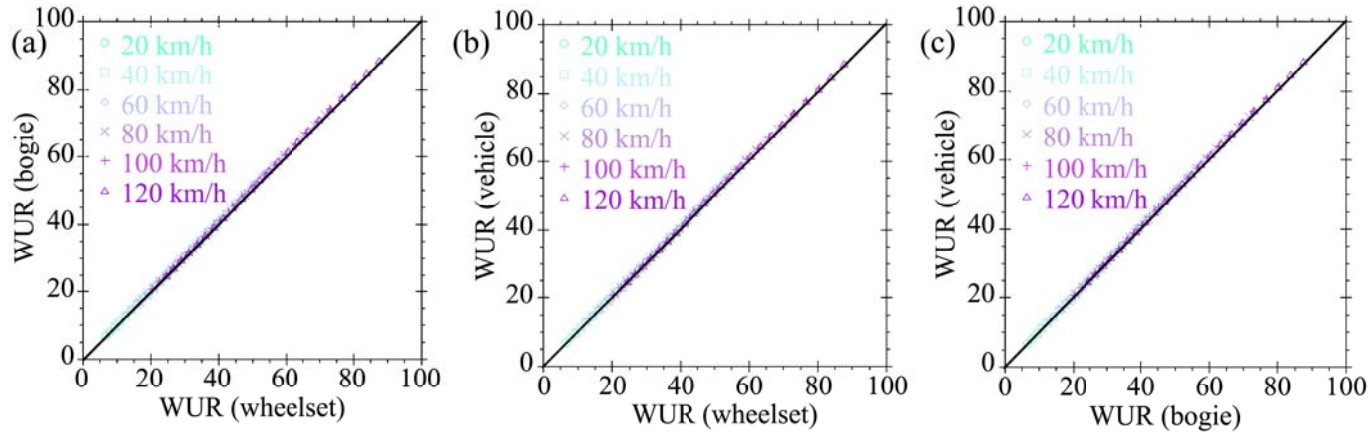

Fig. 12. Comparison of wheel unloading ratio obtained by (a) the first wheelset and two wheelsets of the first bogie, (b) the first wheelset and four wheelsets of the whole vehicle, (c) two wheelsets of the first bogie and four wheelsets of the whole vehicle in quasi-steady winds.

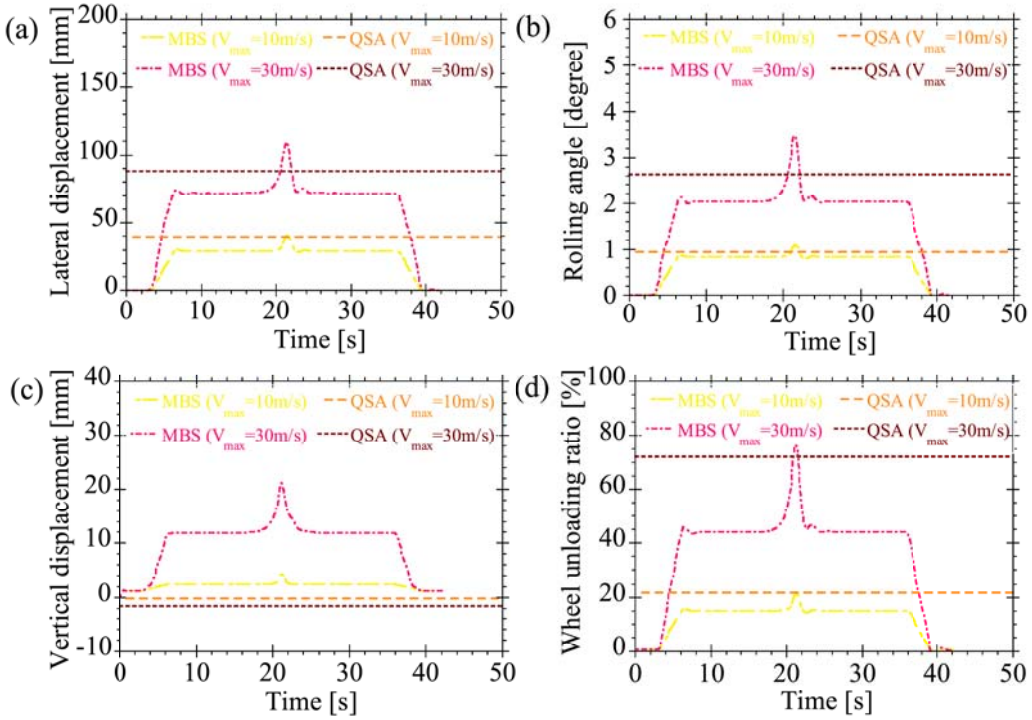

Fig. 14. Comparisons of (a) lateral displacements, (b) vertical displacements, (c) rolling angles of car body and (d) wheel unloading ratios under Chinese hat gust calculated by QSA and MBS.

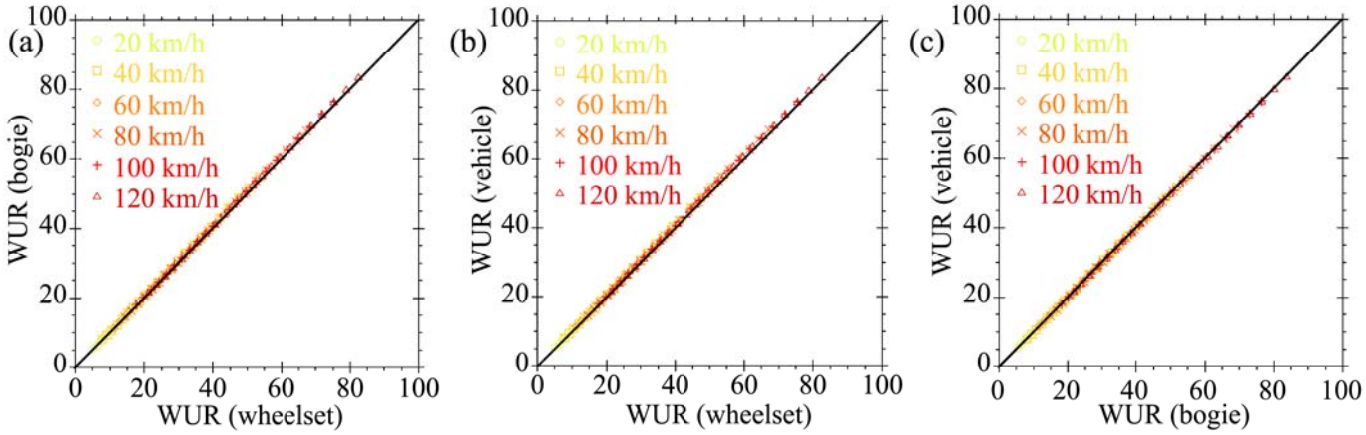

Fig. 15. Comparison of wheel unloading ratio obtained by (a) the first wheelset and two wheelsets of the first bogie, (b) the first wheelset and four wheelsets of the whole vehicle, (c) two wheelsets of the first bogie and four wheelsets of the whole vehicle in Chinese hat gust.

Compared to experimental data, the linear lateral acceleration model proposed by Hibino et al. (2010b) was found to overestimate the effects of track irregularities at high train velocities and underestimate them at low velocities. This indicates that using the linear model to predict critical wind curves at low train velocities may be unsafe. In this study, a non-linear lateral acceleration model is proposed, which maintains a constant value after the train velocity exceeds 20 km/h. This model encompasses most of the measured data, except for several points likely influenced by substructures. The experimental data were collected along tracks with turnouts, bridges, and level crossings, which can cause high lateral accelerations, particularly at high velocities. Therefore, the non-linear model is deemed more accurate for evaluating the effects of track irregularities under normal operational conditions.

Additionally, the percentage of wheel unloading induced by cross-winds and the effects of track irregularities are examined in Fig. 18. For the non-linear lateral acceleration model (NLLAM), the percentage of wheel unloading due to track irregularities is approximately 15 %, slightly exceeding the 10 % value specified in the European code (EN 14067-6, 2010). However, when using the linear lateral acceleration model (LLAM), the wheel unloading ratio induced by track irregularities increases with train velocity, reaching around 23 % at 120 km/h - significantly higher than the European code's recommended value. This suggests that the LLAM overestimates the effects of track irregularities, rendering it conservative. Conversely, at a train velocity of 20 km/h, the LLAM indicates a wheel unloading percentage of 3.8 %, which is about one-third of the value specified in the European code. This underestimation poses a potential danger to railway vehicles even at lower velocities, highlighting the limitations of the linear model in accurately assessing the effects of track irregularities.

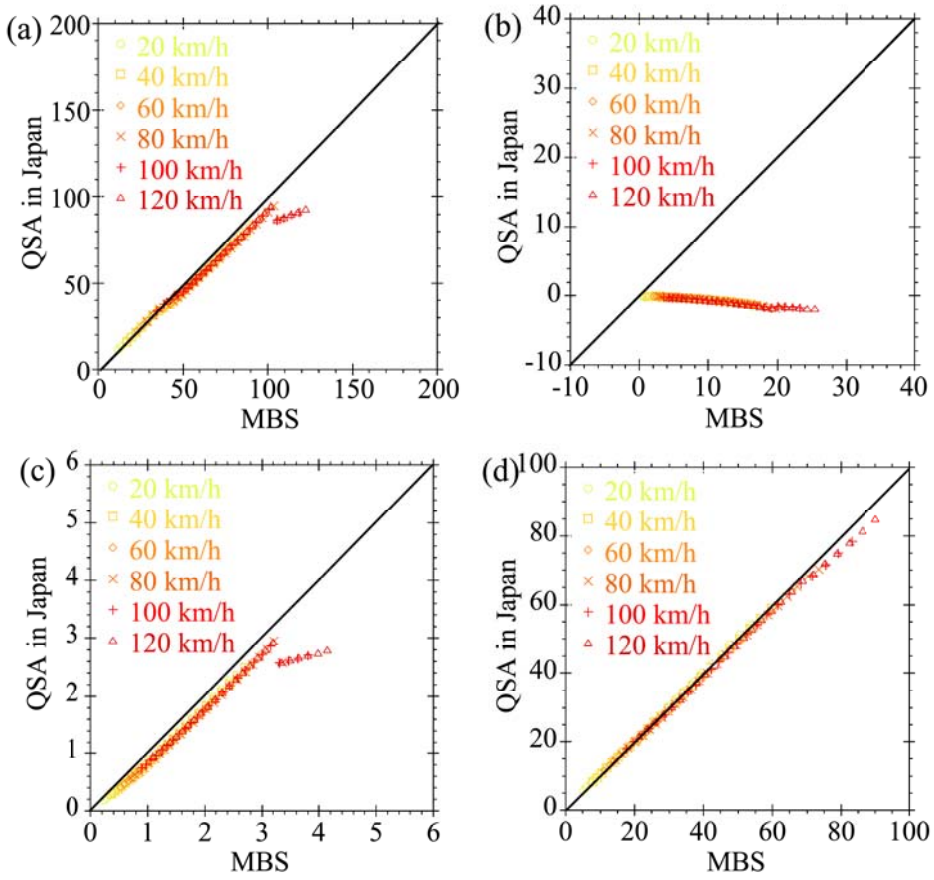

Fig. 16. Comparisons of (a) lateral displacements, (b) vertical displacements, (c) rolling angles of car body and (d) wheel unloading ratios calculated under Chinese hat gust winds by QSA and MBS.

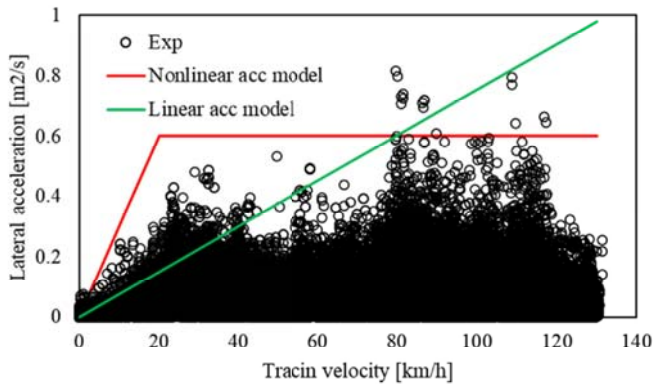

Fig. 17. The lateral acceleration models to consider the effect of track irregularities.

3.3. Comparison of different evaluation criteria

The evaluation criteria for the crosswind stability of railway vehicles across different regions are examined. Initially, the wheel unloading ratio and overturning coefficient, calculated under quasi-steady winds and Chinese hat gust conditions, are compared in Fig. 19. It is observed that these two values are closely aligned at lower wind speeds, with their differences increasing initially and then decreasing as wind speed rises. This variation is primarily attributed to the term $F_L P_L$ in the denominator of Eq. (23). At low wind speeds, the lift force is minimal, rendering $F_L P_L$ negligible. As wind speed increases, the wheel loading on the windward side diminishes and the lift force increases, causing $F_L P_L$ to rise initially before decreasing. Additionally, it is noted that the wheel unloading ratio consistently exceeds the overturning coefficient under both quasi-steady wind and Chinese hat gust conditions.

The evaluation criteria for crosswind stability in Europe and China are further examined, with track irregularities neglected. Initially, the European standard considers a wheel unloading ratio reaching 90 % as the critical value. Both the wheel unloading ratio and overturning coefficient are compared under quasi-steady winds and the Chinese hat gust model in Fig. 20. The analysis reveals that the overturning coefficient is 2 % smaller than the wheel unloading ratio. However, the overturning coefficient significantly exceeds the critical value defined by the Chinese standard, indicating that the Chinese standard is more conservative in evaluating the crosswind stability of railway vehicles than the European standard. Similarly, Fig. 21 compares the wheel unloading ratio and overturning coefficient when adopting the Chinese standard, which considers an overturning coefficient reaching 80 % as the critical value. Under this standard, the wheel unloading ratio is considerably lower than 90 %.

3.4. Comparison of CWC evaluated by different national standards

The characteristic wind curves of railway vehicles, evaluated according to different regional standards, are compared in Fig. 22. It is observed that the CWC evaluated in Europe is slightly higher than that in China, primarily due to differences in the critical values. This indicates that the Chinese standard is more conservative compared to the European standard. In Japan, the characteristic wind speed is significantly higher than in Europe at lower train velocities but much lower than in Europe at higher train velocities. This discrepancy arises because the linear lateral force model underestimates the effects of track irregularities at lower train velocities while overestimating them at higher

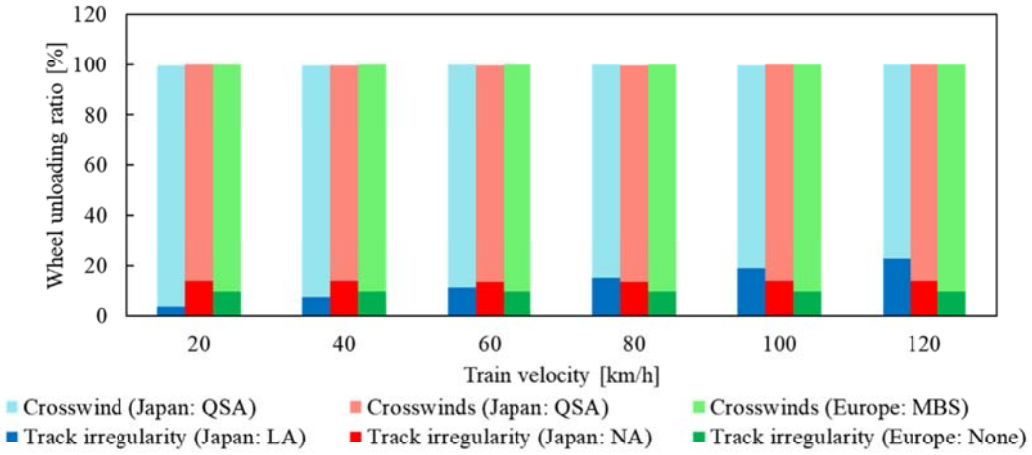

Fig. 18. Percentage of wheel unloading induced by crosswinds and the effects of track irregularities in Japan (Hibino et al., 2010b) and in Europe (EN 14067-6, 2010).

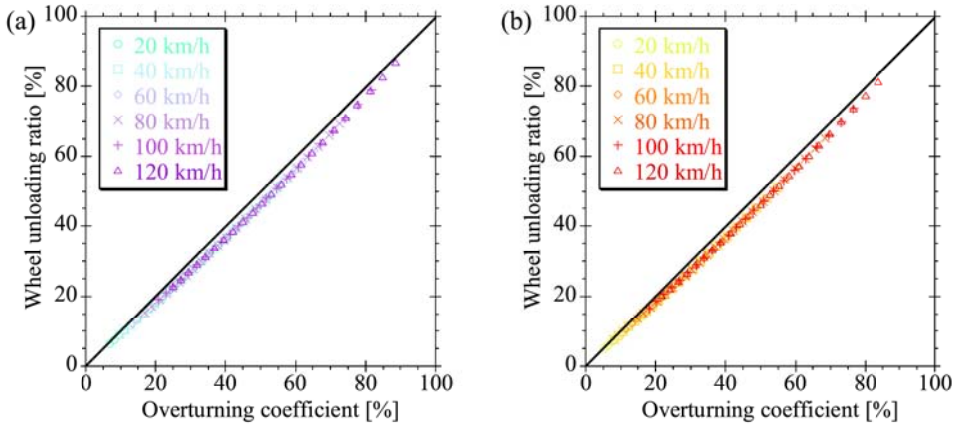

Fig. 19. Relationship between wheel unloading ratio and overturning coefficient: (a) in quasi-steady winds and (b) in the gust model.

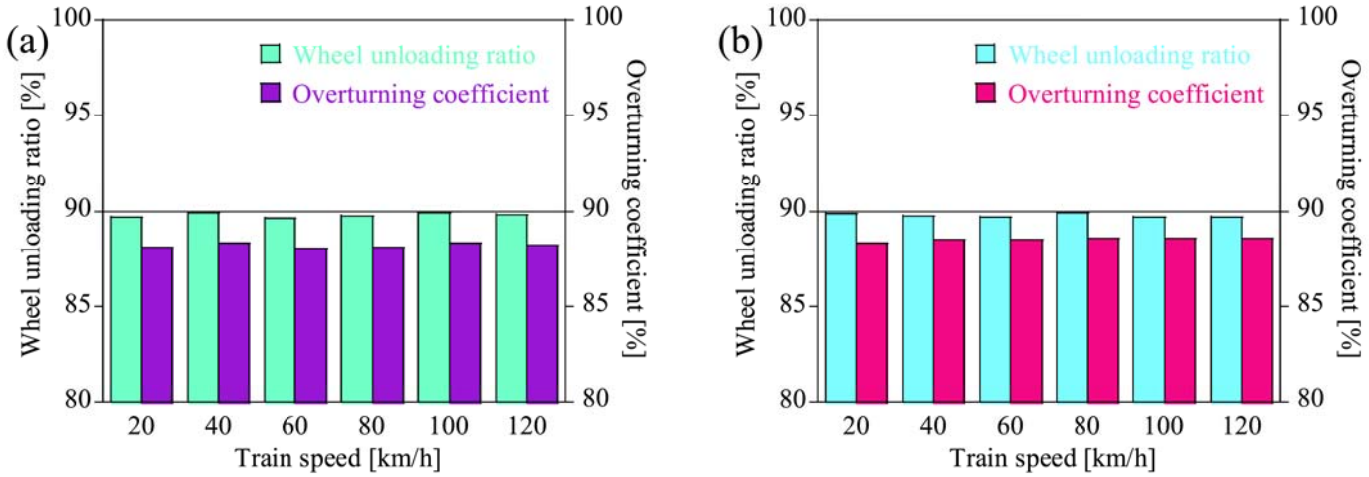

Fig. 20. Variation of overturing coefficient with train speed as the wheel unloading ratio approaches the critical value (90 %): (a) in quasi-steady winds and (b) in the gust model.

velocities. Consequently, the Japanese guideline is non-conservative at lower train velocities but conservative at higher ones. Additionally, the non-linear lateral acceleration model proposed in this study is considered, revealing that the CWC is similar to that in Europe.

It is also noted that the characteristic wind speeds are higher under Chinese hat gust conditions compared to quasi-steady winds. This is because the maximum wind speed is low-pass filtered by centered moving average method, resulting in the actual wind speed acting on the railway vehicle being lower than the maximum wind speed of the Chinese hat gust. Therefore, the characteristic wind speeds are higher.

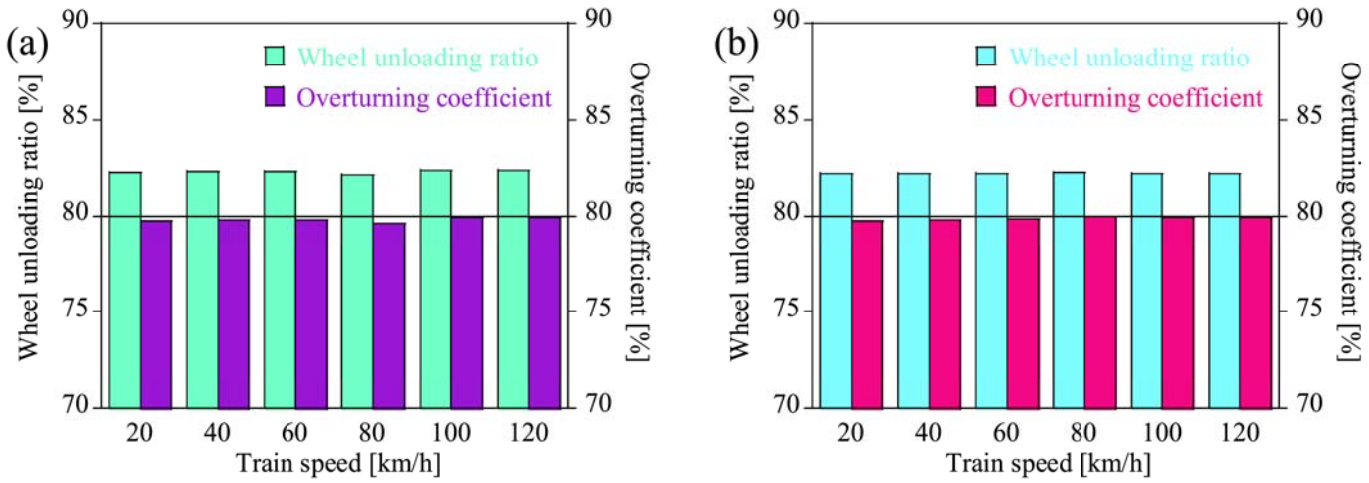

Fig. 21. Variation of wheel unloading ratio with train speed as the overturing coefficient approaches the critical value (80 %): (a) in quasi-steady winds and (b) in the gust model.

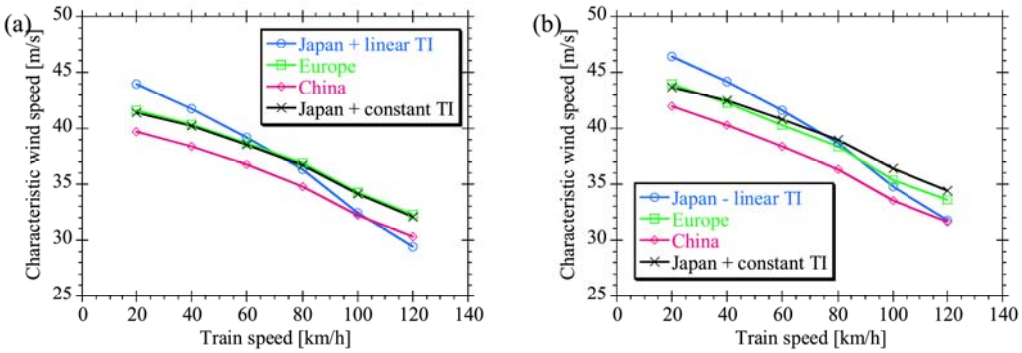

Fig. 22. CWC evaluated by different methods: (a) in steady and (b) gust winds.

3.5. Recommendations for the evaluation of crosswind stability of railway vehicle using different national standards

As railway networks expand globally, particularly with the construction of high-speed lines, ensuring the safety of railway vehicles under crosswind conditions has become increasingly critical. To address this, a generalized evaluation framework is essential. This study compares the evaluation methods and criteria outlined in the railway safety standards and regulations of China, Europe, and Japan, highlighting their respective strengths and limitations, as shown in Table 4.

Notably, Japan's QSA employs a simplified 3-degree-of-freedom (DoF) model, which is computationally efficient and provides reliable results under quasi-steady wind conditions. In contrast, MBS with 27–42 DoFs, offer higher accuracy but with increased complexity. Concerning track irregularities, the linear lateral acceleration model prioritizes safety at high train speeds while overlooking risks at lower speeds. The non-linear acceleration model, based on field test data, offers a more realistic representation of lateral acceleration across varying speeds. While the safety margin approach simplifies the consideration of track irregularities, determining an exact value remains challenging. Regarding the safety criteria, the wheel unloading ratio is more suitable, as it is always larger than the overturning coefficient although this difference becomes smaller under increasing external forces. The Europe's QSA does not consider the track irregularity, but the critical value is 0.90, which is smaller than 1.0 used in the Japan's QSA.

This study also offers key recommendations for evaluating the crosswind stability of railway vehicles.

(a) The QSA method, as employed in Japan, is effective for assessing crosswind stability under a quasi-steady wind conditions due to its simplicity and acceptable accuracy. However, it is not

Table 4
Summarization of the strength and limitation of different models.

		Strength	Limitation
Train model	QSA in Japan	• 3 DoFs, simple and fast • Acceptable results	• Less accurate in gust winds
	MBS	• 27–42 DoFs • Accurate	• Complex
Track irregularity	Linear lateral acceleration model	• Conservative at high train speed	• non-conservative at low train speed
	Non-linear lateral acceleration model	• The lateral acceleration can be determined by field tests	• Slightly complex
	Safety margin	• Simple	• This value should be accurately determined
Criteria	Wheel unloading ratio	• Suitable	–
	Overturing coefficient	• Close to wheel unloading ratio as the external forces increases	• Always smaller than wheel unloading ratio

recommended for evaluating the safety of railway vehicles in the unsteady wind conditions, such as tornado-induced winds.

(b) The effect of track irregularities for crosswind stability evaluations can be modeled either through a non-linear lateral acceleration approach or by applying a safety margin. Current standards that do not consider non-linear lateral acceleration suggest a 10 %–20 % safety margin for the wheel unloading ratio, while the standards that consider non-linear lateral acceleration recommend no safety margin

(c) The wheel unloading ratio is a more appropriate metric for assessing crosswind stability compared to the overturning coefficient. This is because the wheel unloading ratio tends to be larger, providing a more conservative evaluation, although this difference becomes smaller under increasing external forces.

4. Conclusions

In this study, the crosswind stability of railway vehicles, evaluated according to different national standards, is compared. A non-linear acceleration model is proposed to accurately assess the effects of track irregularities. The following conclusions are drawn.

1. Crosswind responses of railway vehicles subjected to quasi-steady winds and gust winds are calculated using both QSA and MBS. It is found that QSA underestimates the wheel unloading ratio of railway vehicles by approximately 3 %, as the external forces increase beyond a certain threshold in quasi-steady winds, due to its neglect of the vertical degree of freedom of the car body. This underestimation is more pronounced under Chinese hat gust conditions, owing to the additional dynamic amplification effects.
2. A simple non-linear model is proposed to simulate the effects of track irregularities when assessing train crosswind stability. This model is validated through field tests. The effects of track irregularities calculated by the non-linear lateral acceleration model align with the European code (EN 14067-6, 2010), while the linear lateral acceleration model overestimates these effects at higher train velocities and underestimates them at lower velocities.
3. Comparisons of crosswind responses of commuter trains under quasi-steady winds and Chinese hat gusts, considering different national standards, reveal that the Japanese guideline is more stringent at high train velocities but more lenient at lower velocities. Compared to the European standard, the Chinese standard is more conservative, with the characteristic wind speed being approximately 2 m/s lower than that calculated by the European standard.
4. Characteristic wind speeds evaluated under Chinese hat gust conditions are around 2.4 m/s higher than those obtained under quasi-steady winds. This is because the maximum wind speed is low-pass filtered by the centered moving average method, meaning the actual wind speed acting on the railway vehicle is lower than the maximum wind speed of the Chinese hat gust.

CRediT authorship contribution statement

Dongqin Zhang: Writing – review & editing, Writing – original draft, Visualization, Validation, Software, Data curation. **Takeshi Ishihara:** Writing – review & editing, Supervision, Resources, Methodology, Investigation, Conceptualization.

Declaration of competing interest

The authors declare that they have no known competing financial interests or personal relationships that could have appeared to influence the work reported in this paper.

Data availability

The authors do not have permission to share data.

Acknowledgements

This study is carried out as a joint research program supported by East Japan Railway Company and the authors would like to acknowledge the support from Dr. Yayoi Misu and Dr. Yosuke Nagumo for providing the field tests.

Appendix A. Validation of the train model

To explore the dynamic response of a commuter rail subjected to natural wind conditions (Ishihara et al., 2021), field tests were conducted by East Japan Railway Company using the E233 series commuter train, widely operated within the Tokyo Megalopolis in Fig. A1(a). The test site featured an embankment-based substructure and a curved track with a radius of 600 m and a cant of 85 mm. Eight strain gauges, positioned equidistantly along the track, captured the wheel load distribution as the train passed. Simultaneously, wind speeds were monitored using anemometers positioned on both sides of the track, enabling the measurement of crosswinds from either direction. The experimental setup is illustrated in Fig. A1(b) and A1(c), where a tangent track is depicted for clarity.

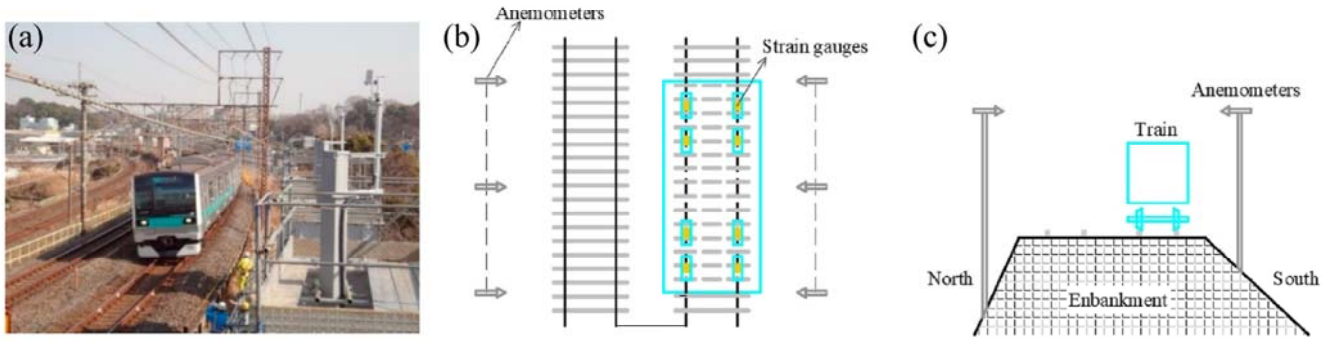

Fig. A1. (a) The E233 commuter rail; (b) configuration of the field test at the top view; (c) and at the front view.

Fig. A2 compares the predicted wheel unloading ratios from both QSA and MBS with the experimental data, encompassing a total of 200 data points. The predictions from both methods demonstrate strong alignment with the measured values. The discrepancies observed between the numerical predictions and experimental data are primarily attributed to uncertainties in track irregularities. Notably, the average wheel unloading ratio

predicted by the multibody simulations exceeds the experimental data by approximately 2 %, while QSA predictions show a 3 % overestimation. These results suggest that both methods yield remarkably consistent estimates of wheel unloading ratios under natural wind conditions. The slight deviations, in the range of 2–3 %, are likely influenced by the track cant, which significantly impacts the excessive centrifugal forces exerted on the railway vehicle.

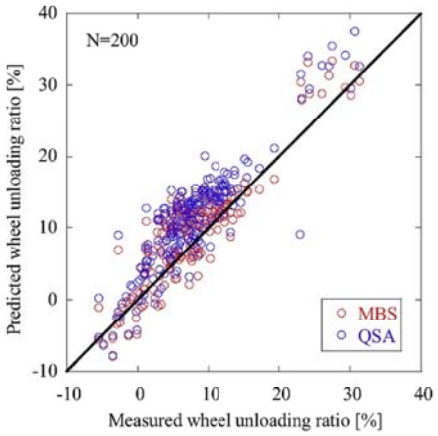

Fig. A2. Comparisons of wheel unloading ratio obtained by measurements and predictions.

References

Akiko, O., Sadaharu, S., Yayoi, M., Youichi, Y., Kenji, H., 2015. Lateral acceleration for evaluation of railway vehicle against crosswind. 22th Rail Tec Symp 1123.

ARAIC, 2008. The Railway Accident Investigation Report: RA2008-4. Japan.

Baker, C., 2013. A framework for the consideration of the effects of crosswinds on trains. J. Wind Eng. Ind. Aerod. 123, 130–142.

Baker, C., Cheli, F., Orellano, A., Paradot, N., Proppe, C., Rocchi, D., 2009. Cross-wind effects on road and rail vehicles. Veh. Syst. Dyn. 47, 983–1022.

Claus, H., Schiehlen, W., 1998. Modeling and simulation of railway bogie structural vibrations. Veh. Syst. Dyn. 29, 538–552.

Diedrichs, B., Ekequist, M., Stichel, S., Tengstrand, H., 2004. Quasi-static modelling of wheel-rail reactions due to crosswind effects for various types of high-speed rolling stock. Proc. Inst. Mech. Eng. - Part F J. Rail Rapid Transit 218, 133–148.

EN 14067-6, 2010. Railway applications - aerodynamics - Part6: requirements and test procedures for cross wind assessment. BS EN 14067-6:2010.

GB5599-85, 1985. Railway Vehicles - Specification for Evaluation the Dynamic Performance and Accreditation Test.

Heleno, R., Montenegro, P.A., Carvalho, H., Ribeiro, D., Calcada, R., Baker, C.J., 2021. Influence of the railway vehicle properties in the running safety against crosswinds. J. Wind Eng. Ind. Aerod. 217, 104732.

Hibino, Y., Kanemoto, H., Shimomura, T., Tanifuji, K., 2010a. Safety evaluation of railway vehicle against crosswind applying a full-vehicle simulation model. Trans. Jpn. Soc. Mech. Eng. Ser. C 76, 3066–3076.

Hibino, Y., Shimomura, T., Tanifuji, K., 2010b. Full-scale experiment on the behavior of a railway vehicle being subjected to lateral force. J. Mech. Syst. Transp. Logist. 3, 35–43.

Ishihara, T., Zhang, D., Nagumo, Y., 2021. Numerical study of dynamic response of railway vehicles under tunnel exit winds using multibody dynamic simulations. J. Wind Eng. Ind. Aerod. 211, 104556.

Liu, D., Wang, Q., Zhong, M., Lu, Z., Wang, J., Wang, T., Lv, S., 2019. Effect of wind speed variation on the dynamics of a high-speed train. Veh. Syst. Dyn. 57, 247–268.

Liu, D., Wang, T., Liang, X., Meng, S., Zhong, M., Lu, Z., 2020. High-speed train overturning safety under varying wind speed conditions. J. Wind Eng. Ind. Aerod. 198, 104111.

Misu, Y., Ishihara, T., 2018. Prediction of frequency distribution of strong crosswind in a control section for train operations by using onsite measurement and numerical simulation. J. Wind Eng. Ind. Aerod. 174, 69–79.

Misu, Y., Ishihara, T., 2012. Prediction of aerodynamic coefficients considering the train speed. J. of Wind Eng., JAWE 37 (4), 117–123.

Montenegro, P.A., Carvalho, H., Ortega, M., Millanes, F., Goicolea, J.M., Zhai, W., Calçada, R., 2022. Impact of the train-track-bridge system characteristics in the runnability of high-speed trains against crosswinds - Part I: running safety. J. Wind Eng. Ind. Aerod. 224, 104974.

Nagumo, Y., Ishihara, T., 2019. A study of crosswind resistant performance of train cars considering uncertainties of acting forces. J. Wind Eng., JAWE 44 (4), 90–104.

Sesma, I., Vinolas, J., San Emeterio, A., Gimenez, J.G., 2012. A comparison of crosswind calculations using a full vehicle and a simplified 2D model. Proc. Inst. Mech. Eng. - Part F J. Rail Rapid Transit 226, 305–317.

Su, D., Fujino, Y., Nagayama, T., Hernandez, J.Y., Seki, M., 2010. Vibration of reinforced concrete viaducts under high-speed train passage: measurement and prediction including train–viaduct interaction. Struct. Infrastruct. Eng. 6, 621–633.

Thomas, D., Diedrichs, B., Berg, M., Stichel, S., 2010. Dynamics of a high-speed rail vehicle negotiating curves at unsteady crosswind. Proc. Inst. Mech. Eng. - Part F J. Rail Rapid Transit 224, 567–579.

Zhai, W., Xia, H., Cai, C., Gao, M., Li, X., Guo, X., Zhang, N., Wang, K., 2013. High-speed train–track–bridge dynamic interactions – Part I: theoretical model and numerical simulation. Int. J. Rail Transp. 1, 3–24.

Zhang, D., Ishihara, T., 2022. Numerical study of tornado-induced unsteady crosswind response of railway vehicle using multibody dynamic simulations. J. Wind Eng. Ind. Aerod. 222, 104919.

Zhang, D., Liu, B., Liang, Y., Jiang, W., Gao, H., Zhang, J., Hu, G., 2024. Numerical study of dynamic amplification factor and characteristic wind curves of high-speed train in tornado-like vortices. J. Wind Eng. Ind. Aerod. 247, 105707.

Zhang, D., Zhong, M., Hu, G., Xiao, Y., 2023. Numerical study of the unsteady crosswind response of high-speed train under local structure-induced unsteady winds by MBS. Eng. Struct. 281, 115788.

Zhang, N., Tian, Y., Xia, H., 2016. A train-bridge dynamic interaction analysis method and its experimental validation. Engineering 2, 528–536.